

ZDZISŁAW BOGDANOWICZ*, DOROTA KOCAŃDA *^{a)}, JANUSZ TORZEWSKI*

APPLYING FRACTOGRAPHIC ANALYSIS FOR THE EVALUATION OF THE EFFECTS OF VARIABLE-AMPLITUDE LOADS ON FATIGUE CRACK GROWTH RATES FOR THE 2024-T3 ALUMINIUM ALLOY

The present paper investigates the effects of variable-amplitude loads on fatigue crack growth rates for the 2024-T3 aluminium alloy on the basis of microfractographic analyses and its capacity to reconstruct load-time histories of failed components. For this purpose, there were applied three different variable-amplitude load sequences with single and multiple overloads and underloads. Subsequently, images of fatigue striations on components' fracture surfaces were examined. The aforementioned loads were employed when simulating fatigue crack behaviour in aeronautical alloys.

1. Introduction

Learning the effects of variable-amplitude loads on fatigue crack growth rates as well as the feasibility of load-time history reconstruction of a failed component on the basis of fractographic analyses has been well-known and used in practice for many years. For the aforementioned purpose, one analyses characteristic features of components' fracture surfaces, namely macroscopic bench marks, as well as fatigue striations in relation to applied loads. Nevertheless, fatigue striations may not be noticeable on fracture surfaces in many cases, which may be related to the types of applied loads or tested materials. Furthermore, the 'one cycle – one striation' relation may only be satisfied in the central part of the crack growth curve. Results of numerous investigations indicate that the growth rate estimated from striation spacing is higher at the initial stage of crack growth and lower at its final stage in comparison

* Military University of Technology, Str. Gen. S. Kaliskiego 2, 00-908 Warszawa, Poland, E-mail: zbogdanowicz@wat.edu.pl, ^{a)} dkocanda@wat.edu.pl – correspond. author, jtorzews-ki@wat.edu.pl

with the rate determined by means of other methods [1]. It is not a rule, of course. For instance, mutual correspondence between the crack growth rates was observed for the 2024-T3 aluminium alloy at constant-amplitude loading in the whole range of crack growth [2]. In the paper by Wanhill [3], it was pointed out that the micrographs taken from the fracture surfaces of 2024-T3 test samples, which were subject to a simulated load spectrum, depicted the load history correctly. Furthermore, the characteristics of the abovementioned fracture surfaces were similar to the ones of the actual structure subject to service loading. The bands lying between the noticeable fatigue striations corresponded to 5000 flights. Service loading was distinctly marked on the fracture surface of the AA7010 aerospace aluminium alloy in the form of systems of fatigue striations [4]. The experimentally determined crack growth rate for the A2017-T3 aluminium alloy under a three-step varying load was compared with the rate estimated from striation spacing [5]. Relatively good conformity between the abovementioned rates was obtained for two load sequences. Results obtained in the case of the third load program were completely discrepant. Microfractographic analysis was employed in order to investigate the influence of the applied load sequences on crack growth rates for the 2024 alloy subject to different surface treatments [6]. The results of the experiment enabled a unique discrimination of interaction effects depending on applied loads and changes concerning fatigue striations' formation. The effect of hydrogen environment embrittlement on fatigue crack growth behaviour in six aerospace aluminium alloys, including the 2024-T3 alloy, was the subject of the work [7]. An extensive research in the aforementioned field was conducted under the conditions of time-dependent hydrogen exposure, time-dependent cyclic deformation in gaseous, aqueous environments and in ultra-high vacuum. A SEM micrograph of the 2024-T3 alloy that was derived from a transition zone revealed a quasi-cleavage mechanism of cracking in vacuum and a subsequent appearance of fatigue striations when the cracking process proceeded in moist air. Fatigue striations were not observable in 7075-T3 alloy plates with semi-elliptical notches that were subject to constant-amplitude tension [8]. However, the presence of fatigue striations was observed after overloads in the basic load spectrum had been applied.

The importance of fractography in supporting the analysis of failed components in actual structures was pointed out by J. Schijve in Ref. [9] and at the ECF-14 conference [10]. Peculiar requirements of aircraft components related to fatigue failure invite the need to scrutinize fatigue crack propagation in aerospace aluminium alloys under different types of load-time histories. For this reason, special skills are required for finding correlation between the images of fracture surfaces and the accumulated fatigue failure caused by the

applied load. The 'one cycle – one striation' relation was examined in Ref. [9] in order to determine crack growth rates for different types of simulated service loading. Then, the relation was presented in diagrams of growth rates versus number of cycles. It should be mentioned that the publications which discuss the abovementioned problem provide both positive and negative opinions on the ability of fractography to reconstruct load-time histories of failed components. Surprising results were obtained in Ref. [11] when investigating in situ small crack behaviour in the 2024-T351 polycrystalline alloy under tension and under bending. Fracture surface analysis proved a plastic mechanism of cracking. However, fatigue striations were not evident on the surface.

The effects of load interaction on fatigue crack growth behaviour when applying single or multiple overloads are widely reported in the publications. For load histories that included overloads, the appearance of fatigue striations on fracture surfaces depends on particular combinations of load parameters as well as materials. When relating crack growth to load parameters, one needs to take into account the number and frequency of overloads applied during basic loading (BL) as well as the ratio of an overload stress OLR, which is defined below. Still, it can happen that multiple overloads, which interrupt baseline cycles, do not lead to the appearance of striations on a fracture surface. The aforementioned case is often observed for aluminium alloys and is reported in the studies mentioned below. An insignificant effect of overloads on crack growth rates occurred in aluminium alloys such as 2024-T3 [12], 7075 and 8090 [13] under an aircraft service spectrum as well as in seven other aerospace aluminium alloys [14]. The phenomenon found confirmation on the plots of crack growth rates also for 2524-T3 Al-clad aluminium sheets and in titanium alloys [15] subject to the Embraer simulated service operation. In contrast, stronger interaction effects on crack growth behaviour occurred in 2024-T3 when a single overload was applied and repeated time and time again until failure [12]. The aforementioned results found confirmation also in our research conducted on the 2024-T3 aluminium alloy.

Therefore, there is a considerable interest in evaluating the capacity of the models for predicting fatigue crack growth. For this purpose, there was developed a research program for fatigue crack growth behaviour of thin 2024 sheets subject to two different heat treatments, namely T3 and T2, under variable-amplitude sequences that are typical of helicopter utilisation in order to support analytical and numerical modelling of crack growth in lower wing skins [16]. It was found that 2024-T2 specimens exhibited slightly longer crack propagation lives compared to 2024-T3 Alclad specimens. Accuracy and reliability of the prediction models commonly used by FASTRAN,

NASGRO, CORPUS and AFGROW were tested with a view to evaluating graphs of crack lengths versus numbers of cycles as well as the distributions of the ratios of the numbers of cycles assessed in experimental tests as opposed to the calculated ones, for particular crack growth intervals. The comparison results showed big discrepancies between the abovementioned graphs. Retardation and acceleration effects caused by the applied overloads were distinctly marked on the experimental graphs. Trends in crack growth behaviour were illustrated only by three predicted graphs. The worst results were obtained by means of AFGROW. A crack growth analysis concerning the 7075-T6 aluminium alloy subject to service loading, which was conducted with the help of identical numerical programs mentioned in Ref. [16], is the subject of work [17]. A broad review of fatigue crack growth behaviour in metal materials, including aluminium alloys, under both simple and complex variable-amplitude load sequences as well as the presentation of fatigue crack growth prediction models are included in monograph [18].

Fractographic analysis is also used in order to study fatigue failure processes in actual structures and to reconstruct the service loads of failed components. The importance of fractography in supporting the analyses was pointed out in the books published both by V.C. Ivanova et al. [19] and J. Schijve [10]. Nevertheless, fatigue striations may not be noticeable on fracture surfaces in many cases, which may be related to the types of applied loads or tested materials. Therefore, load reconstruction might be impossible. This phenomenon is often observed for aluminium alloys. On the other hand, peculiar requirements of aircraft components related to fatigue failure inspire researchers to study fatigue crack propagation in aerospace aluminium alloys under different types of loading in order to scrutinize striation systems formed on fracture surfaces. In the case of load histories involving overloads, the formation of fatigue striations on fracture surfaces depends on particular load parameters and materials. It can happen that multiple overloads which interrupt baseline cycles do not lead to the appearance of striations on fracture surfaces. The aforementioned results were also confirmed in our research carried out for the 2024-T3 aluminium alloy [20]. Fractography was also used for analysing fatigue crack initiation and growth in aeronautical aluminium alloy rivet-joints [22], [24] as well as for evaluating the effects of amplitudes and load rates on energy dissipation in the case of aluminium alloys subject to cyclic torsions [23].

The present work presents the fatigue crack growth behaviour of the 2024-T3 Alclad aluminium alloy when applying three variable-amplitude (VA) load sequences while simulating the fatigue behaviour of aeronautical alloys. Moreover, the work discusses the problem of reconstructing load-time histories of components on the basis of microfractographic analyses.

2. The material and experiment procedure

The material used in tests was a 3 mm thick 2024-T3 Alclad aluminium alloy sheet. The clad layer was 120 μm thick. The central crack tension specimens (CCT) were 400 mm long and 100 mm wide (Fig. 1). In order to make it easier to compare fatigue properties depending on the sheet rolling direction, specimens were cut longitudinally (LT) and transversely (TL) to the rolling direction. Mechanical properties were in the following ranges: the ultimate tensile stress was 447-466 MPa, the yield stress was 303-335 MPa and elongation was 21-24%. The highest values of the aforementioned properties were observed for LT specimens. Average grain diameters in the clad layer were 85-89 μm , whereas in the matrix material, they were 29-35 μm in the case of LT specimens and 18-25 μm in the case of TL specimens. In specimens subject to constant-amplitude (CA) cyclic tension ($R = 0.1$), crack growth rates were found to be independent of the cutting direction.

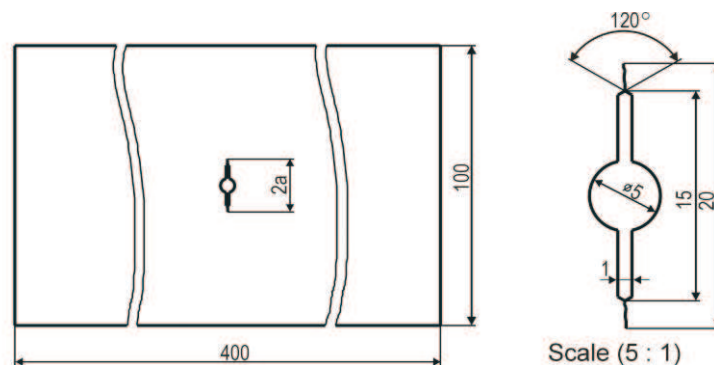


Fig. 1. Specimen geometry (dimensions in mm)

For the purpose of crack propagation tests, specimens were provided with a central notch consisting of a through-thickness hole that was 5 mm in diameter, a 5 mm long through-thickness saw cut and a 2.5 mm long pre-crack on each side of the hole. The initial crack length was $2l = 20$ mm, measuring from tip to tip of the pre-crack. All fatigue tests were carried out under controlled cyclic loading at the frequency of 2 Hz.

In order to check the capacity of microfractographic analysis for reconstructing load-time histories for the 2024-T3 aluminium alloy, there were applied three variable-amplitude (VA) load programs (Figs 2, 3 and 4) that differed in the level of load sequence complexity. The aforementioned programs are applied in crack propagation tests of the lower skins of aircraft wings subject to flight simulation loads. The first program, called OVL, was proposed by J. Schijve. It includes a load sequence of 211 cycles with few overloads, as shown in Fig. 2.

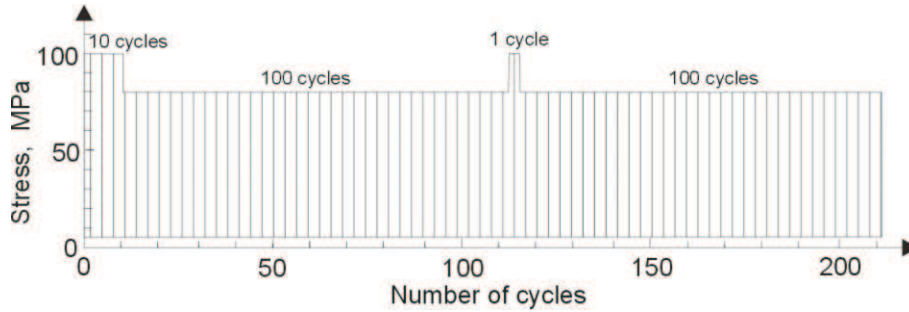


Fig. 2. A load sequence with overloads (the OVL program)

The base constant-amplitude load (CA) is interrupted by 10 overloads; then, there is applied a similar single overload which is followed by 100 base cycles. The aforementioned 10 overloads are also preceded by 100 basic cycles. Maximum stress at overload is $S_{max} = 100$ MPa and the overload rate is $OLR = 1.266$. Overload rate (OLR) is defined as $OLR = (K_{OL} - K_{min, BL}) / (\Delta K_{BL})$, where K_{OL} , $K_{min, BL}$ and ΔK_{BL} are the overload stress intensity factor, the baseline minimum stress intensity factor and the baseline stress intensity factor range respectively. The second load program, called LHL-100 (Fig. 3) corresponds to 100 flights and its load cycles are arranged in 13 blocks. Each block has the same maximum and minimum loads but the ranges of the stress amplitudes and the numbers of cycles depend on stress levels which are numbered from 1 through 7. The total number of cycles in one LHL-100 program is 2400.

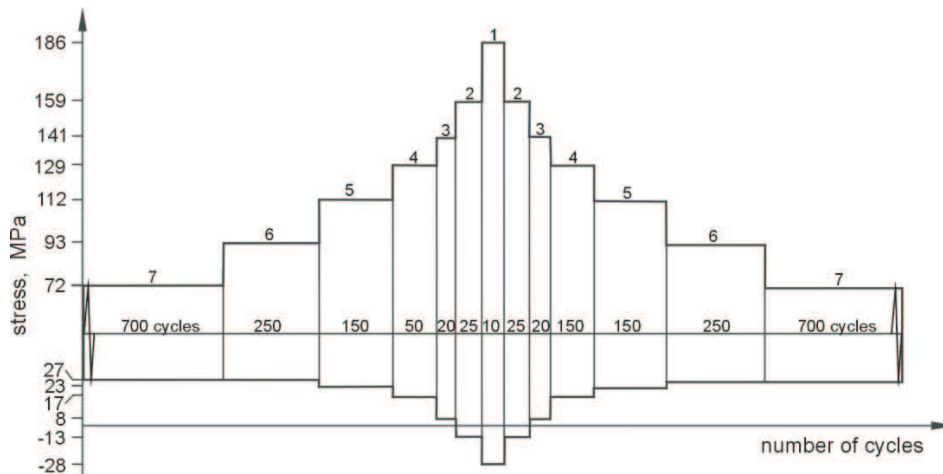


Fig. 3. A schematic of the LHL-100 block program

The third VA load program, called FBF (flight-by-flight), consists of two blocks of cycles, namely 'Flight A' and 'Flight B'. The schematic of

the FBF program is presented in Fig. 4. The 'Flight A' block is repeated nine times, whereas the 'Flight B' block occurs only one time per one FBF load sequence. One load sequence numbers 240 cycles. Both 'Flight A' and 'Flight B' are of the low-high-low type with spike overloads/underloads of varying magnitudes. Ten FBF sequences correspond to one LHL-100 block program.

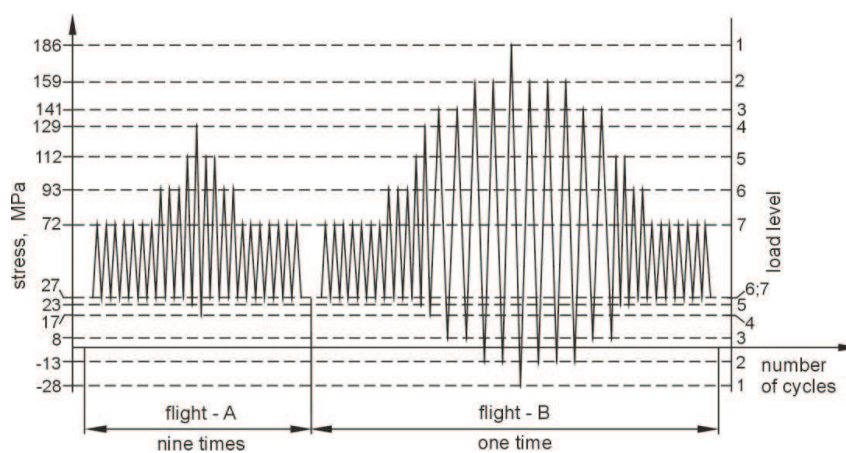


Fig. 4. A schematic of the FBF sequence of cycles

All load programs were being repeated until a specimen's failure. The X-ray diffraction method revealed the presence of compressive residual stresses of 400 MPa in the Alclad layers of LT and TL specimens both with and without pre-cracks. Crack length was monitored visually with the use of a magnifying glass. For the purpose of the visual recording of the crack tip positions, a line scale was inscribed on specimens' surfaces along the crack path. The accuracy of crack length readings was 0.2 mm. Additionally, the crack tip area was recorded with a video camera. The load sequence effect on crack growth rate was analysed by means of a transmission electron microscope (TEM). Prior to the TEM observations, plastic replicas taken from fracture surfaces were shadowed with platinum.

3. Results and discussion

Fatigue crack growth under variable-amplitude loading

It should be emphasized that the considerations concerning fatigue crack growth behaviour under variable-amplitude loading (VA) refer only to long cracks. An analysis of the obtained results will be discussed separately for each load test.

3.1 Test results obtained for the OVL program

Fatigue crack growth behaviour of the 2024-T3 aluminium alloy under the OVL program (Fig. 2) is analysed on the basis of Figs 5 and 7 as well as the image presented in Fig. 6, which illustrates a fracture surface with fatigue striations that appeared as a result of applying the load program being discussed. In Fig. 5, experimental data concerning surface crack growth rates obtained for the OVL program was compared with the data concerning surface crack growth rates obtained under CA loads. As expected, multiple overloads applied in a baseline stress amplitude caused a significant decrease in crack growth rates. However, retardation and acceleration effects corresponding to particular blocks of overloads are not clearly visible in the experimental graphs in Fig. 5. It probably resulted from the methodology used when measuring crack lengths on specimens' surfaces.

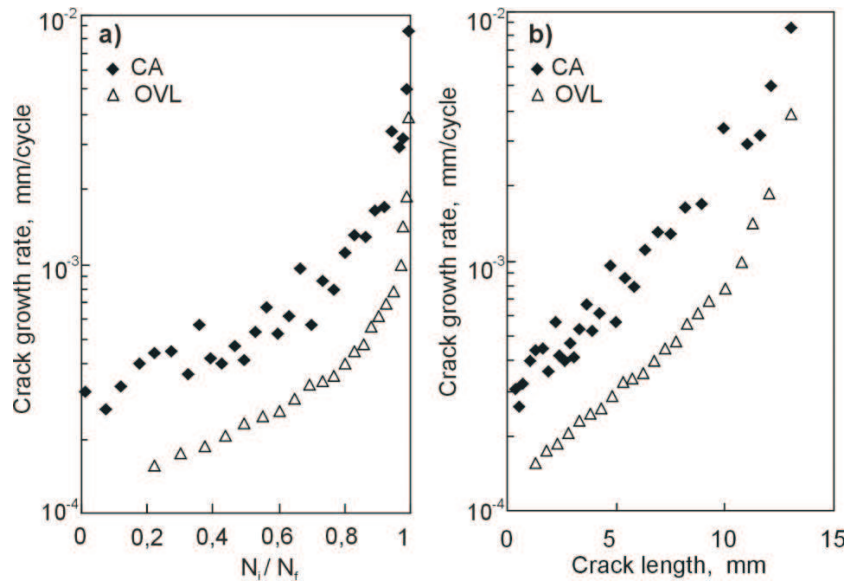


Fig. 5. Experimental curves of fatigue crack growth rates versus crack lengths (a) and cycle ratios N_i / N_f (b) under constant-amplitude (CA) and program loading (OVL), respectively

Effects of the applied overloads on crack growth rates can be examined by analyzing a TEM micrograph that originates from points located at different distances from the notch bottom. A sample TEM micrograph with striations, which is shown in Fig. 6, corresponds to a half of the load sequence.

In the image, from left to the right side, one can easily identify a band with 10 thick striations corresponding to 10 applied overloads, a band with 100 thin striations corresponding to 100 base cycles and a single thick striation created by a single overload. The ten overloads caused a significant

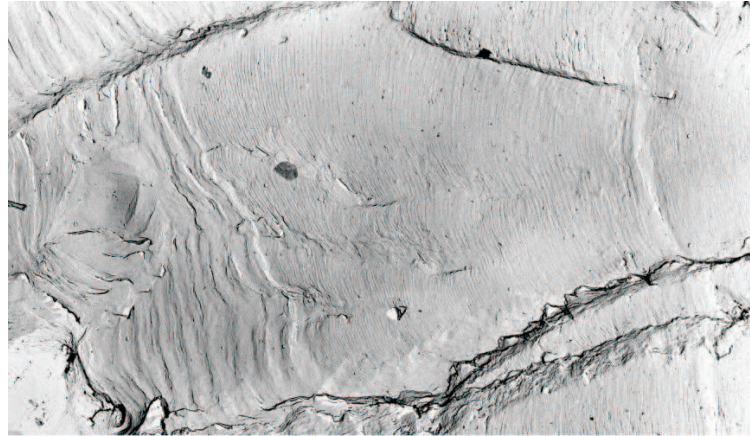


Fig. 6. A TEM micrograph illustrating a system of fatigue striations created during the OVL load test

retardation effect, which occurred immediately after the overloads had been applied. When approaching the single thick striation, striation spacing gradually increases due to crack growth rate acceleration. The TEM micrograph makes it possible to accurately reconstruct the loading history as well as the changes in crack growth rates in the 2024-T3 alloy under the OVL loading. The curves of local crack growth rates affected by particular sequences of cycles were determined on the basis of striation spacing. The crack growth rates versus crack lengths are shown in Fig. 7.

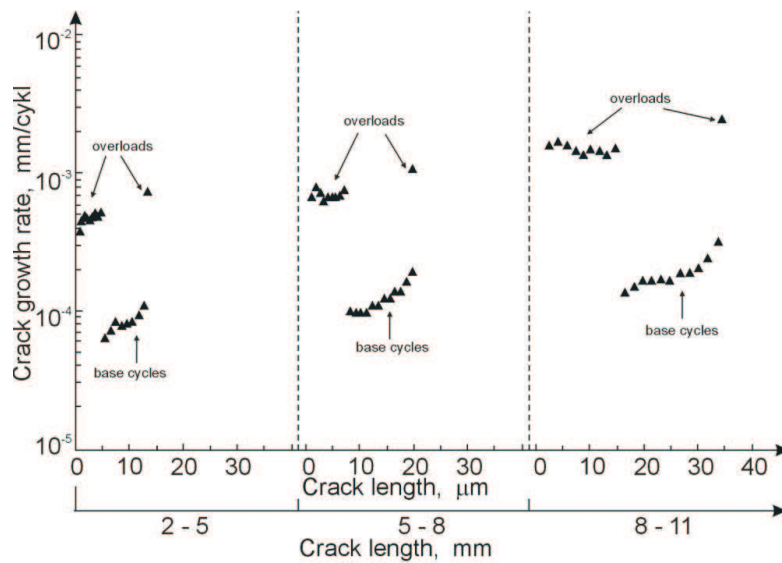


Fig. 7. Local crack growth rates corresponding to OVL loads versus crack lengths; (see text for explanation)

Crack length intervals (in millimetres), measured from the pre-crack, are marked on the lower horizontal axis whereas crack length increment (in micrometers) estimated from striation spacing is marked on the upper horizontal axis. As shown in the diagram, ten overloads caused an initially high crack growth rate. However, under successive overloads, the crack growth rate decreased and eventually dropped by almost two orders of magnitude. Subsequently, the crack growth rate gradually increased in the phase corresponding to 100 base cycles and there were periods characterized by constant crack growth rates. Applying a single overload in base cycles resulted in either a sudden crack growth rate jump or its rapid drop by one order of magnitude. Load interaction lead to a delayed retardation of crack growth and then to its gradual increase in the phase corresponding to the application of successive 100 base cycles. The crack growth retardation was caused by the plastic zone created by overloads, which was located ahead of the crack tip. Compressive stresses acted in the aforementioned zone, in the area of the crack tip. As observable in the diagram, multiple overloads cause more significant crack growth rate retardation than a single overload. One can observe a significant increase in crack growth rates as the number of load sequences in the test increases.

3.2. Test results for the LHL-100 block program loading

Figure 8 illustrates fatigue crack growth rates estimated for the LHL-100 program as well as the CA test versus surface crack lengths for specimens cut longitudinally (LT) (Fig. 8a) and transversely (TL) (Fig. 8b) to the sheet rolling direction.

Data marked by opened (white) symbols represents visually recorded (OPT) surface crack lengths. Data marked by filled-in-black symbols represents crack depths measured fractographically (striation spacing on fracture surfaces) by means of a scanning electron microscope (SEM). The above mentioned data was compared with the data concerning surface crack growth rates under CA loads.

Discrepancies between the two VA data sets are small similarly to the ones in CA tests. A similar trend was observed for TL specimens, though crack growth rates were slightly higher in the case of TL specimens than in the case of LT specimens. All VA test results fall significantly below the CA test data (Figs 8a and 8b) since the LHL-100 block program considerably reduces the crack growth rate in the most part of the specimens' lifetime. In the final part of the fatigue life the VA crack growth rate reaches the CA rate.

The effect of load interaction on crack growth rates corresponding to the particular load blocks is not clearly visible in the experimental graphs.

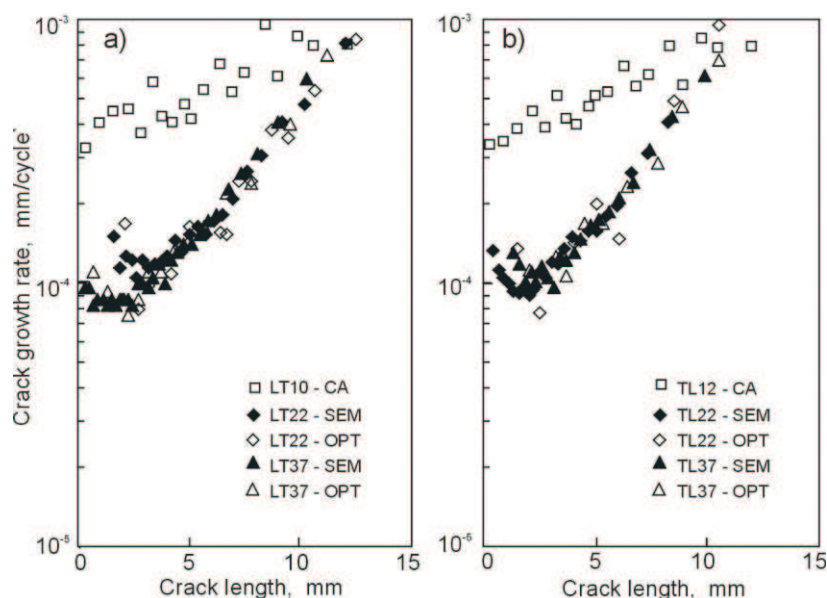


Fig. 8. A comparison of crack growth rates corresponding to the LHL-100 block program and to CA loading versus crack lengths for LT specimens (a) and for TL specimens (b); surface crack rates recorded optically (OPT) and crack depth rates measured by means of SEM

In order to examine the aforementioned effect more closely TEM or SEM micrographs ought to be analysed. Sample TEM micrographs, which are presented in Fig. 9, illustrate systems of fatigue striations that correspond to the descending and ascending parts of one full block program observed on fracture surfaces at the distance of 2 to 8 mm from the notch bottom.

The images mentioned above illustrate particular crack length ranges measured from a fatigue pre-crack front, which are respectively equal to 2-5 mm (Fig. 9a), 5-8 mm (Fig. 9b) and 8-11 mm (Fig. 10). In the case of specimens loaded according to the LHL-100 program, they are the repeating patterns of fatigue striations which are observable under the TEM up to the length of 12 mm from the mechanical notch. The systems of fatigue striations can be observed in the increasing part of the spectrum at levels 3-2-1 and in the decreasing part of the spectrum at levels 1-2-3. At load levels 7-6-5-4 and 4-5-6-7, there are merely trace quantities of striations, which indicates an arrest of crack growth or its propagation at a very low rate.

The nature of the transition of the crack path from the increasing to the decreasing part of the spectrum can be observed in the images. The transition may manifest itself in a step and a narrow strip (Figs 9a and 10) or in very narrow bands (Fig. 9b). The transitions is observed in central parts of the images. The transitions manifested themselves in steps and smooth bands with either no fatigue striations or merely traces of striations. The width of

particular crack surface segments are approximately $3\ \mu\text{m}$ in Figs 9a and 9b and about $1.5\ \mu\text{m}$ in Fig. 10, respectively. In accordance with the number of cycles in particular load levels (Fig. 3), the analyzed bands correspond to 2300 load cycles (load levels 4-5-6-7), while the striated segments correspond to 100 load cycles (load levels 1-2-3). The images in Figs 9 and 10 indicate the crack tip closure or the propagation of the crack at a very low rate, which constitutes a proof of the crack growth retardation on a microscopic scale. The increasing striation spacing, especially in the image in Fig. 10, indicates an increase in the crack growth rate. The gradual increase or decrease in striation spacing in particular series may be ascribed to particular levels in the load spectrum.

Local changes in the crack growth direction, as observable in Fig. 9a and to some extent in Fig. 10, were caused by second phase inclusions or cavities left after them, which can be observed in the right part of the image in Fig. 9a, whereas a quite large pyramid-shaped inclusion, which can be observed in the central right part of the image in Fig. 9b, did not change the cracking direction. An identical inclusion observable in the left part of the image in Fig. 10 affected the direction of cracking to a small extent, however, it interrupted the continuity of the occurrence of wide striations.

The images of fracture surfaces obtained by means of the SEM are less clear and more difficult to interpret. Exemplary images are presented in Fig. 11. The images illustrate fracture surfaces of LT specimens. Extensive and somewhat jagged fracture surfaces as well as second phase intermetallic inclusions and cavities left after the removal of the inclusions disturb the uniformity of cracking and deteriorate the legibility of the images. The image in Fig. 11a was taken at the distance of $a = 1.5\ \text{mm}$ from the fatigue pre-crack while the image in Fig. 11b was taken at the distances of $a = 3.5\ \text{mm}$. The image in Fig. 11a shows two series of clearly evident thick and thin striations, which correspond to the number of overload cycles in stress blocks in accordance with the load spectrum presented in Fig. 3. Striation spacing in the series of thick striations in Fig. 11a is $3.3\ \mu\text{m}$, while in Fig. 11b it is invariable and is approximately equal to $2.8\ \mu\text{m}$. The presented images of thick and thin fatigue striations correspond well with the distribution of measuring points in the diagrams of crack growth rates in LT specimens presented in Fig. 8a. In the range of crack lengths of up to $4.5\ \text{mm}$, at the beginning, the crack growth rate was higher, which lasted for a short period of time. Subsequently, the crack rate either dropped or settled at an invariable level. Next, the crack growth rate was increasing quite rapidly until the specimen's failure.

It is interesting that the consistency of crack growth rates occurs both on a macroscopic and microscopic scale. The former is related to spacing between

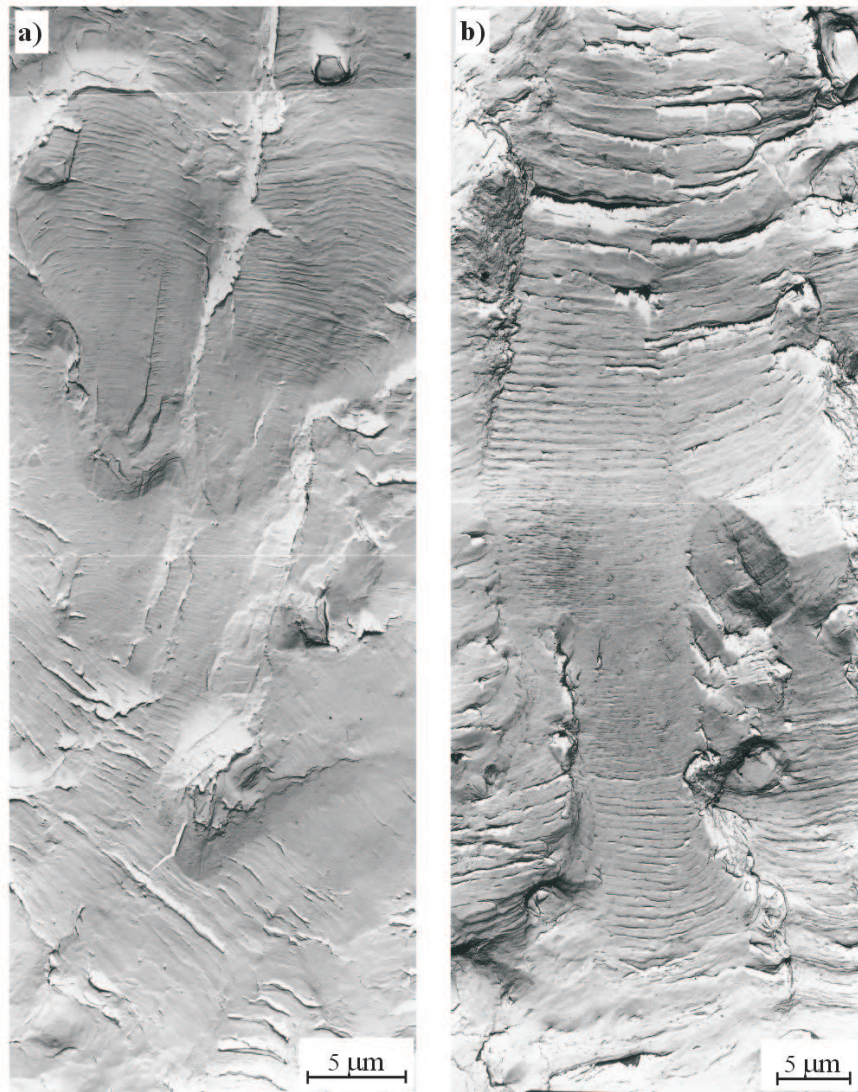


Fig. 9. Patterns of fatigue striations on the fracture surfaces of 2024-T3 alloy LT specimens observed with the use of the TEM within the decreasing and increasing parts of stress spectra in the lengths ranges of 2-5 mm (a) and 5-8 mm (b) from the pre-crack front; (see text for explanation)

fatigue lines, whereas the latter is related to fatigue striation spacing, which differ in terms of dimensions by 2-3 orders of magnitude. The consistency, or rather macroscopic analogy, is repeated in very narrow bands with overload striations which correspond to 10, 25 or alternatively 20 load cycles (load

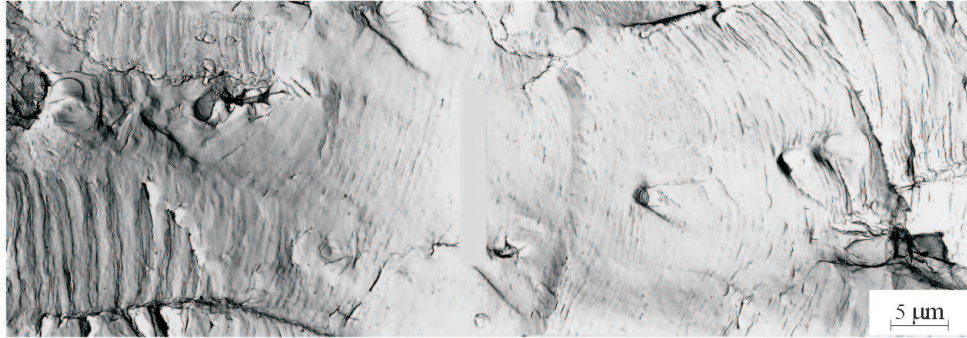


Fig. 10. A pattern of fatigue striations on the fracture surface of the 2024-T3 alloy LT specimen observed with the use of the TEM within decreasing (left side of the image) and increasing (on the right side) parts of the LHL-100 stress spectrum in the length ranges of 8-11 mm from the pre-crack front; (see text for explanation)

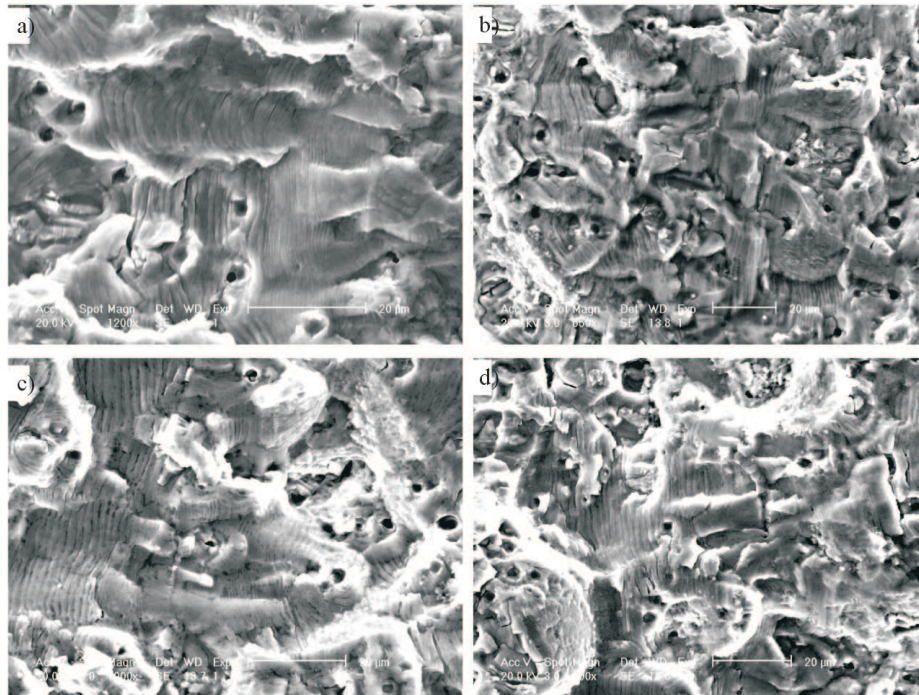


Fig. 11. Fracture surfaces of the 2024-T3 aluminium alloy for the LHL-100 stress spectrum observed with the use of the SEM at the distance of 1.5 mm (a), 2.2 mm (b), 3.5 mm (c) and 4.5 mm (d) from the pre-crack front; (see text for explanation)

levels 1-2-3). The analysis of fracture surfaces under the TEM and partially under the SEM confirmed the occurrence of temporary crack growth delay

and crack closure caused by overload cycles in the stress spectrum. The importance of microfractographic analysis carried out with the use of electron microscopes (the TEM microscope in particular) should be underscored. Appropriate preparation of fracture replicas is crucial for the tests carried out with the use of the TEM. As a general rule, making replicas is a very laborious task. Working out the proper technique of making replicas led to obtaining clear and legible images, as in Figs 9 and 10. Whereas the analysis by means of the SEM is characterized by great simplicity since crack surfaces can be observed directly under the microscope, which is a great convenience. On the other hand, there is usually a decrease in the quality and the precision of the images obtained by the SEM. Comparing the images in Figs 9, 10 and 11, it is easy to notice the difference in quality between the images obtained by means of the TEM and the ones obtained with the use of the SEM. The patterns of striations noticeable in the fracture surfaces in the images obtained with the use of the TEM and presented in Fig. 9 and 10, made it possible to determine changes in crack growth rates in the spectrum, that is, on a microscopic scale. The changes are illustrated in a diagram in Fig. 12.

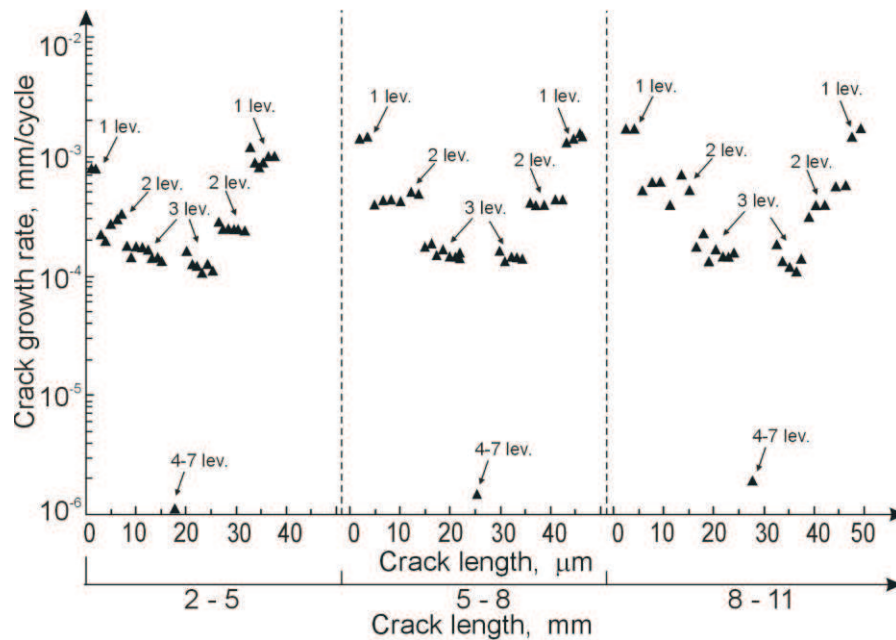


Fig. 12. Local crack growth rates corresponding to the LHL-100 stress spectrum versus crack lengths; (see text for explanation)

Similarly as for the OVL program, two scales were used, namely the upper scale relating to striation spacing and the lower scale relating to the

point at which the fracture surface for the TEM analysis was taken. Crack growth rates determined from the striation spacing data and corresponding to particular load levels of the LHL-100 spectrum are marked in the diagram. The patterns of striations are characteristic of spectra in the range of crack lengths of 2-11 mm. The high initial crack growth rate, which manifested itself in thick fatigue striations, decreased significantly from 10^{-3} mm/cycle to 10^{-4} mm/cycle, subsequently, it decreased rapidly to 10^{-6} mm/cycle. The decrease was manifested in single measuring points at the bottom part of the diagram in Fig. 12. The drop in crack growth rate in specimens encompassed three orders of magnitude. Then, there occurred a comparably rapid and gradual increase in crack growth rate also by three orders of magnitude. The phenomenon of the rapid decrease and increase in crack growth rate occurred in the middle part of each crack length range, which can be observed in the diagram in Fig. 12. It manifested itself in narrow bands with either no striations or traces of striations, which can be noticed in the central parts of the images in Figs 9 and 10. The microfractographic analysis proved that short loading cycle sequences (as regards the number of cycles) and successive loading blocks which occur at relatively short intervals reduce the possibility of a complete reconstruction of a loading spectrum on the basis of the microfractographic analysis of failed components.

3.3. Test results for the FBF load program

The FBF load program (Fig. 4) has a common load spectrum with the LHL-100 block program but differs from the latter in the arrangement and number of cycles in particular blocks. The FBF sequence includes only one spike overload/underload of the highest stress ratio of $S_{UL\ min}/S_{OV\ max} = -0.15$. Effects of the applied load on crack growth behaviour can be examined by analyzing experimental results presented in Figs 13 and 16 as well as TEM micrographs presented in Fig. 14. In order to verify the results of load tests the curves of crack growth rates versus visually measured surface crack lengths for two LT specimens (Fig. 13a) and two TL specimens (Fig 13b) were compared with the results obtained from the CA test. One might expect that the growth rates under FBF loading were lower than the ones obtained in the CA test.

More details concerning the effect of load on the crack growth behaviour were obtained from TEM micrographs. Exemplary TEM micrographs corresponding to FBF loading are presented in Fig. 14.

Changes in the local crack growth rate within one sequence were estimated cycle by cycle on the basis of TEM measurements taken at different points on a fracture surface. Also the microfractographic analysis by means

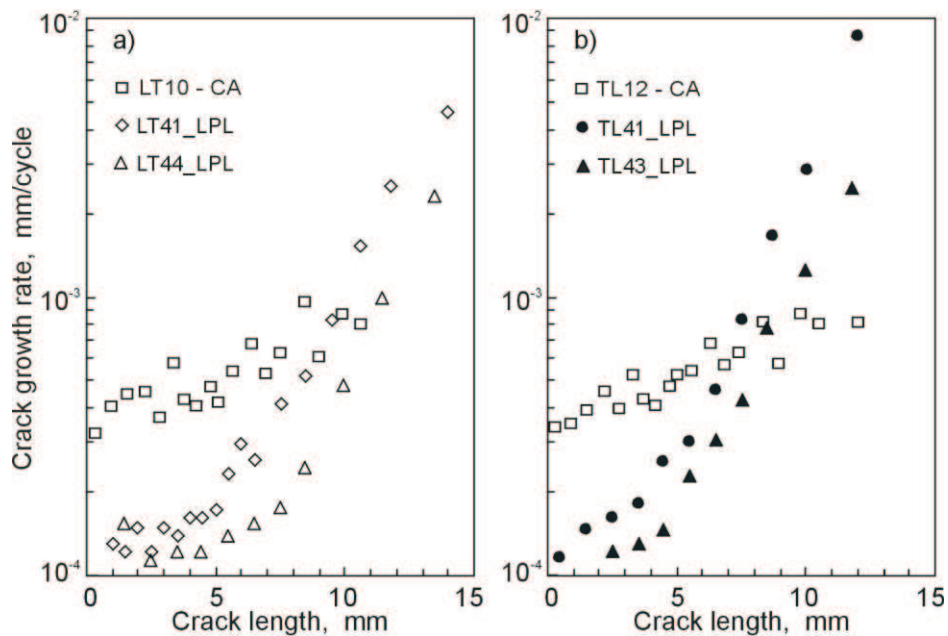


Fig. 13. A comparison of crack growth rates under the FBF sequence of cycles (LPL) and under CA versus measured crack lengths for specimens cut longitudinally (a) and transversely (b) to the sheet rolling direction

of the SEM microscope provided images of the fracture surfaces of specimens subject to FBF loads. Characteristic patterns of fatigue striations on the fracture surface of a 2024-T3 alloy LT specimen can be observed in the image in Fig. 15.

The above image illustrates groups of repeating striations of different widths. The image illustrates fatigue striations corresponding to a complete sequence of stress blocks in the FBF program. The thickest striations can be observed in the centre of the image in Fig. 15a. All of them correspond to the cycle with the highest stress value in the 'Flight-B' block at load level 1. The cycle with the highest stress value in the spectrum (level 1) caused a rapid increase in crack growth rate and a crack increment that manifested itself in the form of a wide flat band between two striations and the next three striations formed as a result of the operation of two cycles and the next three cycles at load level 2 in the 'Flight-B' block. A set of striations of the same width, which can be observed in the central part of the image, corresponds to stress level 4 (both for the 'Flight-A' block and the 'Flight-B' block). A plastic zone created by the highest cycle encompasses 220 striations. The aforementioned number of striations encompasses striations formed during the nine-fold repetition of the 'Flight-A' block and 23 striations

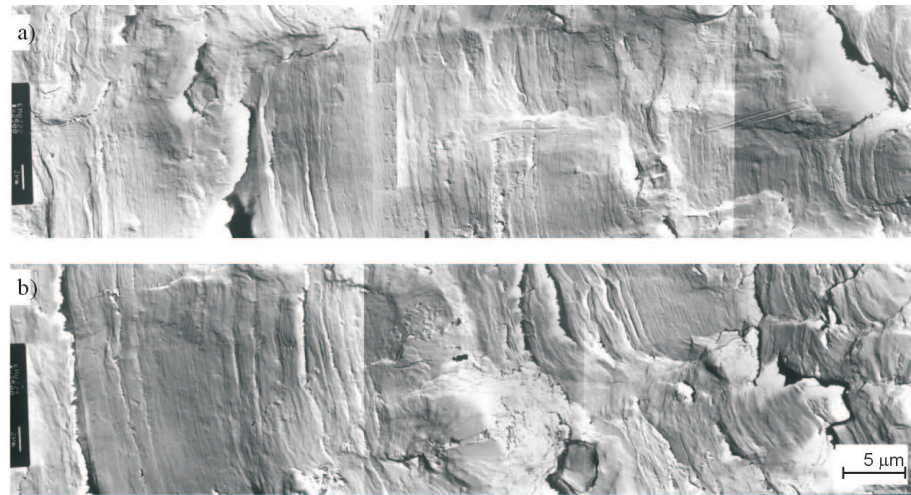


Fig. 14. Patterns of fatigue striations on the fracture surfaces of 2024-T3 alloy LT specimens observed with the use of the TEM within the successive sequences of the FBF program in the length ranges of 2-5 mm (a) and 5-8 mm (b) from the pre-crack front; (see text for explanation)

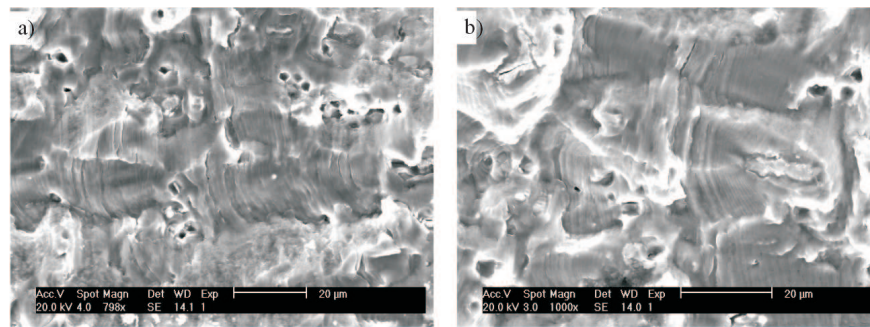


Fig. 15. Fracture surfaces of a 2024-T3 aluminium alloy LT specimen subject to the FBF stress spectrum, observed with the use of the SEM at the distance of 1 mm (a), 2.2 mm (b) from the pre-crack front; (see text for explanation)

formed during the operation of cycles at levels 4 through 7 in the 'Flight-B' block. It denotes that crack growth rate was very low during the operation of 220 cycles in the spectrum. Then, each high-density series of striations, which is noticeable in the images in Figure 15 and on the macrofracture in the form of a fatigue line, consists of 10 striations formed during the operation of 10 cycles at levels 3-2-1-2-3 and 10 striations corresponding to level 4 in a complete FBF program. The diagrams of crack growth rates

(on a microscopic scale) that were estimated on the basis of fatigue striation spacing on the fracture surfaces of specimens (the upper crack length axis in the diagram) are presented in Fig. 16. The sections of fracture surfaces taken at different distances from the mechanical notch (the lower crack length axis in the diagram) were compared. Fatigue striations corresponding to the four highest stress levels in the FBF load spectrum were identified during a microfractographic examination.

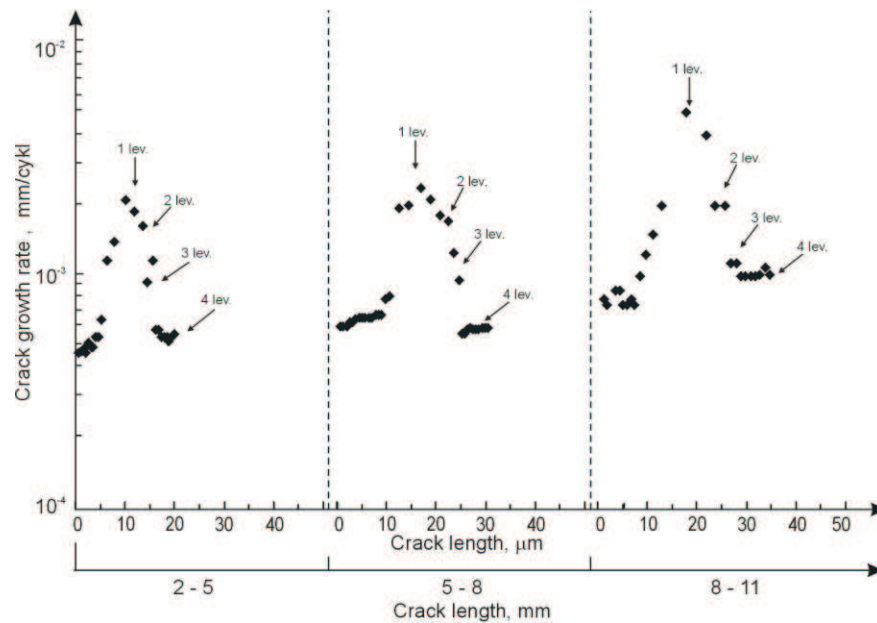


Fig. 16. Local crack growth rates corresponding to the FBF stress spectrum versus crack lengths; (see text for explanation)

Points that correspond to crack growth rates determined from striation spacing and related to the highest load levels in the FBF program were marked in the abovementioned diagram. Data presented in Fig. 16 indicates that the highest spike overload/underload cycle of the first stress level played an important role in the sequence and lead to the formation of the widest striation. On the other hand, unloading reduced the effect of crack retardation. In the case of FBF loading, crack propagation period encompassed only 20 cycles out of 240 cycles that made up the whole sequence. In the micro scale, crack growth rate corresponding to one spike overload/underload cycle was almost three times higher than the one caused by the operation of ten immediately-following spike overload/underload cycles in the LHL-100 program. Finally, the lifetimes of specimens subject to FBF loading were lower than the ones that were tested under the LHL-100 block pro-

gram. In the case of complex VA load sequences with a certain number of immediately-following spike overloads/underloads, the possibility of reconstructing load-time histories on the basis of microfractographic analyses is limited. TEM observations make it possible to identify only a part of striations corresponding to particular cycles in a load sequence. The limited reconstruction possibility results also from short return periods of the investigated load programs. Our research conducted in this field indicates that in the case of simple load programs with blocks of spike overloads/underloads with longer return periods, the correspondence between fatigue striations and relevant load cycles is very good in the whole range of crack lengths.

4. Conclusions

The research on 2024-T3 aluminium alloy sheets was conducted in order to learn more about the effects of variable-amplitude loading with repeated spike overload/underload cycles on fatigue crack growth behaviour. There were analyzed three load sequences, namely a basic OVL load program, the FBF (flight-by-flight) sequence of cycles and the LHL-100 block program that differed from one another in the arrangement and number of overloads of varying magnitudes or spike overload/underload cycles. Obtained results indicate that the first overload/underload cycle in the sequence of either the FBF or the LHL-100 load programs plays a very important role. A single high spike overload/underload cycle in the FBF sequence reduces the effect of crack retardation more than a block with ten immediately-following spike overloads/underloads in the LHL-100 program. As a result, the lifetimes of specimens subject to the FBF loading are shorter than the ones under the LHL-100 block program. The research also proved that short return periods, which are characteristic of variable-amplitude loadings with a certain number of immediately-following spike overload/underload cycles, lead to the limitation of the possibility to accurately reconstruct load-time histories on the basis of microfractographic analyses.

Manuscript received by Editorial Board, May 20, 2009;
final version, December 02, 2009.

REFERENCES

- [1] Kocańda S.: Metal Fatigue. Part III in *Experimental Methods in Mechanics of Solids*. Amsterdam-Oxford-New York, Elsevier, 1990, PWN Warszawa, 1990.
- [2] Kocańda D., Kocańda S., Torzewski J.: Fatigue crack growth rate in 2024-T3 aluminium alloy. *Proc. XIX Symposium on Fatigue and Fracture Mechanics (Zmęczenie i Mechanika Pękania)* Publishing of ATR Bydgoszcz, 2002, pp. 195-202 (in Polish).

- [3] Wanhill R.J.H.: Flight simulation fatigue crack growth guidelines, Proc. Eighth International Fatigue Congress – Fatigue 2002, 2002, Vol. 1/5, pp. 573-584.
- [4] Spence S.H., Williams N.M., Stonham A.J., Bache M.R., Ward A.R., Evans W.J., Hay D., Urbani C., Crawford B.R., Loader C., Clark G.: Fatigue in the presence of corrosion pitting in an aerospace aluminium alloy, *Ibidem*, pp. 701-708.
- [5] Katoh Y., Nakayama H., Tanaka T.: Fatigue crack growth behaviour of aluminium alloy under three-step varying load, *Ibidem*, Vol. 2/5, pp. 1459-1466.
- [6] Sunder R.: An explanation for the residual stress effect in metal fatigue, *Ibidem*, Vol. 5/5, pp. 3339-3350.
- [7] Gangloff R.P.: Environment sensitive fatigue crack tip process and propagation in aerospace aluminium alloys, *Ibidem*, Vol. 5/5, pp. 3401-3430.
- [8] Forth S.C., Keat W.D., Fawrow L.H.: Experimental and computational investigation of three-dimensional mixed-mode fatigue. *Fatigue Fract. Engng Mater. Struct.* 2002, Vol. 25, No 1, pp. 3-15.
- [9] Schijve J.: Fatigue of structures and materials in the 20th century and the state of the art, Proc. 14th Biennial Conference on Fracture – ECF 14, 2002, Vol. III/III, pp. 211-262.
- [10] Schijve J.: Fatigue of structures and materials. Kluwer Academic Publishers, Dordrecht, Boston, London, 2001.
- [11] Zhang X.P., Wang C.H., Ye L., Mai W.: In situ investigation of small fatigue crack growth in poly-crystal and single-crystal aluminium alloys. *Fatigue Fract. Engng Mater. Struct.* 2002, Vol. 25, No 2, pp. 141-150.
- [12] Kermanidis A.T., Pantelakis S.G.: Fatigue crack growth analysis of 2024-T3 aluminium specimens under aircraft service spectra. *Fatigue Fract. Engng Mater. Struct.*, 2001, Vol. 24, pp. 699-710.
- [13] Ranganathan N.: Certain aspects of variable amplitude fatigue, Proc. Eighth International Fatigue Congress - Fatigue 2002, 2002, Vol. 1/5, pp. 613-621.
- [14] Brockenbrough J.R., Bucci R.J., Kulak M., Zonker H.R., Bray G.H., Heinimann M.B., Newman J.C.: Crack growth prediction methods for spectrum loading to support fatigue and durability damage tolerance evaluation. International Committee on Aeronautical Fatigue (ICAF), Fatigue of Aeronautical Structures as an Engineering Challenge, Lucerne, Switzerland, 2003, pp. 14.
- [15] Goncalves W., Pramono A., Chaves C.E.: Embraer new family of jets-meeting the current fatigue and damage tolerance requirements. *Ibidem*, pp. 21.
- [16] Lazzeri L., Ratti G.: Fatigue crack propagation in thin sheets under typical helicopter spectra, Proc. Eighth Int. Fatigue Congress – Fatigue 2002, 2002, Vol. 1/5, pp. 585-592.
- [17] Iyyer N.S., Kwon Y.S., Nam Phan: P-3C crack growth life predictions under spectrum loading. International Committee on Aeronautical Fatigue (ICAF), Fatigue of Aeronautical Structures as an Engineering Challenge, Lucerne, Switzerland, 2003, pp. 18.
- [18] Skorupa M.: Empirical trends and prediction models for fatigue crack growth under variable amplitude loading. Netherlands Energy Research Foundation ECN-R-96-007, 1996.
- [19] Ivanova V., Shaniavsky A. Quantitative fractography. Metallurgy Press, 1988 (in Russian).
- [20] Kocańda D., Kocańda S., Torzewski J. Reconstruction of fatigue crack growth rate for 2024-T3 aluminium alloy sheet on the basis of fractographic analysis. *Archive Mech. Engng*, Vol. LI, No 3, pp. 361-376, 2004.
- [21] Hertzberg R., Deformation and fracture mechanics of engineering materials, Second Ed., 1983.
- [22] Karasiewicz T., Bogdanowicz Z., Polański J.: The influence of amplitude and load rate on the amount of energy dissipation for aluminium alloy subject to cyclic torsion. *Bull. Military University of Technology*, Nr 4, 2007 (in Polish).
- [23] Szymczyk E., Jachimowicz J., Bogdanowicz Z.: Investigations of fatigue crack initiation in rivet-joints. *Scientific Letters of Świętokrzyska Politechnika*, s. Mechanics, 2007 (in Polish).

- [24] Elaboration of the method of aeronautical skin joints lifetime determination taking into account materials and technological features. Sc. Project, Military University of Technology, 2008, Z. Bogdanowicz – leadering (in Polish).

Zastosowanie analizy fraktograficznej do oceny wpływu obciążenia o zmiennej amplitudzie na prędkość zmęczeniowego pęknięcia stopu aluminium 2024-T3

S t r e s z c z e n i e

W pracy przedstawiono wyniki badań fraktograficznych, na podstawie których analizowano wpływ obciążenia o zmiennej amplitudzie naprężeń na prędkość zmęczeniowego pęknięcia stopu aluminium 2024-T3 oraz możliwość rekonstrukcji historii obciążenia zniszczonego elementu konstrukcji. Badania te prowadzono dla trzech widm obciążenia z pojedynczymi i wielokrotnymi cyklami przeciążającymi lub odciążeniowymi. Te widma obciążenia są stosowane wtedy, gdy badany jest rozwój pęknięć w stopach lotniczych. Badania wykazały, że dla tego typu krótkich sekwencji obciążenia cyklicznie powtarzanych aż do zniszczenia elementu nie jest możliwa pełna rekonstrukcja widma obciążenia elementu na podstawie analizy mikrofraktograficznej.